This article has been accepted for publication in a future issue of this journal, but has not been fully edited. Content may change prior to final publication. Citation information: DOI 10.1109/TPEL.2021.3101713, IEEE Transactions on Power Electronics

Hybrid Data-Driven Modeling Methodology for Fast and Accurate Transient Simulation of SiC MOSFETs

Peng Yang, *Student Member, IEEE,* Wenlong Ming, *Member, IEEE,* Jun Liang, *Senior Member, IEEE,* Ingo Lüdtke, Steve Berry, and Konstantinos Floros

***Abstract*—To enable fast and accurate models of SiC MOSFETs for transient simulation, a hybrid data-driven modeling methodology of SiC MOSFETs is proposed. Unlike conventional modeling methods that are based on complex nonlinear equations, data-driven Artificial Neural Networks (ANNs) are used in this paper. For model accuracy, the I-V characteristics are measured in the whole operation region to train the ANN. The ANN model is then combined with behavior-based equations to model the cutoff region and to avoid overfitting the ANN. In addition, the C-V characteristics are modeled by ANNs with a logarithmic scale for accuracy. The proposed model is implemented and simulated in SPICE simulator SIMetrix. The simulation results are compared with experimental results from a double-pulse tester to validate the proposed modeling methodology. The model is also compared with the Angelov model created by the Keysight MOSFET modeling software. The comparison results show that the proposed model is more accurate than the Angelov model. Besides, when compared to the Angelov model, the proposed model requires 30% less computation time when simulating a double pulse tester. In addition, the proposed modeling method also has better adaptability to model different types of SiC MOSFETs.**

***Index Terms*—SiC MOSFET, transient model, hybrid modeling, artificial neural network.**

I. Introduction

SILICON Carbide (SiC) metal-oxide-semiconductor field-effect-transistors (MOSFETs) are gaining popularity in recent years. This is due to the superior material properties of SiC compared to Silicon. For example, SiC features higher switching speed, lower switching losses, higher thermal conductivity and higher operation temperature capability [1]. Such properties help increase power density and efficiency of power electronics converters such as traction inverters and on-board chargers in electric vehicles [2].

This work was supported by the European Commission's Horizon 2020 Research & Innovation Programme (Marie Skłodowska-Curie Actions) through the project "Innovative Tools for Offshore Wind and DC Grids (InnoDC)", under Grant 765585, and the EPSRC "Sustainable urban power supply through intelligent control and enhanced restoration of AC/DC networks", under Grant EP/T021985/1. (Corresponding author: Wenlong Ming)

P. Yang and J. Liang are with School of Engineering, Cardiff University, Cardiff, CF24 3AA, United Kingdom. (e-mail: yangp6, liangj1@cardiff.ac.uk).

W. Ming is with School of Engineering, Cardiff University, Cardiff, and also with Compound Semiconductor Applications Catapult, Newport, United Kingdom. (e-mail: mingw@cardiff.ac.uk).

I. Lüdtke, S. Berry and K. Floros are with Compound Semiconductor Applications Catapult, Newport, United Kingdom (e-mail: ingo.ludtke, steve.berry, konstantinos.floros@csa.catapult.org.uk).

High-power-density design of power electronics converters requires accurate power losses analysis of SiC MOSFETs, especially switching losses [3]. High-speed operation of SiC MOSFETs increases the dv/dt and di/dt of the switching transients [4], which causes electromagnetic interference (EMI) problems to the converters [5]. Although switching losses and EMI can be examined experimentally, it is often required to build multiple hardware prototypes for testing, which is very expensive and time consuming. An alternative approach is computer aided design [6]. Compared to the experimental approach, the computer-aided-design methodology is more time-efficient, as it can be used to simulate the power losses and EMI for converter optimization. However, this approach requires accurate and fast SiC MOSFET model to predict the switching waveforms to nanosecond level accuracy. Such SiC MOSFET model can be also used to optimize the design of gate driver [7], heat sink [8] and EMI filters [9].

Many modeling methods of SiC MOSFETs have been reported in previous literature and a review of SiC MOSFETs model was presented in [10]. The available modeling methods are based on either physics-based, numerical or behavior models. Among them, physics-based and numerical models can provide accurate simulation results based-on the carrier transportation in the channel and drift regions [11], [12]. Physics-based and numerical-based models are built based on the device geometry such as the channel length and width, the thickness of the gate oxide layer and N-drift region, doping concentration of different regions, etc [13]. Therefore, the model built for one device can be extended to another device with different current or voltage levels by adjusting the physical parameters of the model [14]. But these models are complex and have slow computation speed so are not suitable for transient simulation. Also, the information of device geometry is usually not available to users [15]. As a result, they are mostly used at the design stage of SiC MOSFETs [16].

Instead, behavior models are widely used in transient circuit simulation due to their simplicity and fast computation speed [17], which is therefore the focus of this paper. Most existing behavior models are implemented using mathematical equations to match the measured device characteristics, such as I-V and C-V characteristics [18]. Complex nonlinear equations are firstly designed according to the device characteristics. Afterwards, the equation parameters are extracted using mathematical curve fitting methods [19].

This article has been accepted for publication in a future issue of this journal, but has not been fully edited. Content may change prior to final publication. Citation information: DOI 10.1109/TPEL.2021.3101713, IEEE Transactions on Power Electronics

In [7], a SPICE Level 1 behavior model was used to model SiC MOSFETs but the I-V characteristics in the high voltage region were not considered, which deteriorates the model accuracy for transient simulation. To overcome this problem, an improved Angelov model was proposed in [20], in which the I-V characteristics in the high voltage region were used to improve the model accuracy. The Angelov model parameters can be automatically extracted in a commercially available parameter extraction tool (IC-CAP; Keysight Technologies, Inc.) using the Levenberg-Marquardt algorithm [21]. However, the automatically extracted parameters may not be accurate enough and the parameters often need to be manually tuned, which is time-consuming and requires expert experience. Also, some behavior models like the Angelov model [22] have more than 80 parameters, making the parameter extraction very difficult even for users with expert experience. In addition, compared to physics-based and numerical-based models, the behavior models have limited generality due to the lack of physical information. Therefore, if behavior models built for one device are used to model another device with different current or voltage levels, parameters of the models need to be extracted again based on device characteristics.

A new behavior modeling algorithm based on ANNs was proposed in [23]–[25] which aimed to give a simple and fast data-driven method. Thanks to the data-driven approach, such ANN-based models can potentially overcome the aforementioned challenges of the conventional behavior modeling methods. Complex equation design is avoided and the ANN parameters can be extracted easily and automatically by training the ANN using many well-developed toolboxes such as the Neural Net Fitting Toolbox in MATLAB. In addition, ANNs have good adaptability to model SiC MOSFETs with different characteristics because ANNs can approximate any mathematical functions [26]. However, the existing ANN-based modeling methods are only suitable for static simulation but not for transient simulation due to the insufficient training dataset and inaccurate data-driven model.

In this paper, a hybrid data-driven behavior modeling methodology is proposed to achieve fast and accurate transient simulation. At its core, an ANN-based data-driven model is used to model the I-V and C-V characteristics in the whole operation region, which is overlaid with behavior-based equations to accurately model the cutoff region. Two samples of the SiC MOSFET module CAS120M12BM2 were used to validate the proposed modeling methodology on accuracy and repeatability. The training dataset of ANNs were measured from one sample and the transient switching waveforms were measured from another sample. The accuracy of the proposed hybrid modeling method is verified by comparing simulated and measured switching waveforms from the SPICE simulator SIMetrix and a double pulse tester (DPT), respectively. The proposed model is also compared with the Angelov model in [20]. It is shown that the proposed model can achieve $1.5\sim3$ times more accuracy and better adaptability than the Angelov model. Besides, the computation time of the proposed model is compared with the Angelov model through simulating the same DPT circuit in SIMetrix. The runtime of the proposed model is found to be 30% faster than Angelov model.

The main contribution of the paper is that, for the first time, an ANN-based hybrid data-driven modeling method is proposed and verified for accurate transient simulation of SiC MOSFETs. The proposed method improves accuracy of SiC MOSFET models by $1.5\sim3$ times, compared to the widely used Angelov model. It is found that simply using the data measured from a curve tracer to train the ANNs cannot generate an accurate transient model of SiC MOSFET. The accuracy of the model is largely determined by two factors, i.e., high-quality training dataset and proper data-driven model, which are detailed as follows:

1) For the training dataset of the I-V characteristics, compared to existing methods [23], it is identified that the I-V characteristics in the high voltage region (i.e. saturation region up to the maximum DC voltage across the MOSFETs) must be included to obtain accurate simulation results across the whole operation region of SiC MOSFETs in transient simulation.
2) It is identified that a proper data-driven model is critical for accurate modeling of the I-V characteristics. Since the cut-off region of the I-V characteristics is hard to be modeled correctly by a pure data-driven model presented in existing methods, a hybrid data-driven model is proposed to model the cutoff region accurately.
3) The training dataset and proper data-driven model are also identified for the C-V characteristics which are not considered in existing methods. The C-V characteristics are measured in the whole V_{DS} region in logarithmic scale as the training dataset, and logarithmic transformation is applied in ANN models for accuracy.

As a result, the proposed modeling method improves the accuracy of transient simulation, which in turn can be used for accurate analysis of power losses and EMI in computer-aided design of power converters based on SiC MOSFETs.

II. Review of the Existing ANN Model

It was noted in the conclusions of [23] that the existing ANN model is not suitable for transient simulation. In this section, the existing ANN model is reviewed from the structure to the limitations on transient simulation. A 1200V 120A module CAS120M12BM2 from Wolfspeed was selected to facilitate the analysis.

A. Structure of artificial neural network

As shown in Fig. 1, a single-hidden-layer ANN was used to model the I-V characteristics of SiC MOSFETs. The single-hidden-layer ANN consists of an input layer, a hidden layer and an output layer. The input layer has two neurons to receive two input variables: the drain-to-source voltage V_{DS} and gate-to-source voltage V_{GS}. The output layer has one neuron which outputs the drain-to-source current I_{DS}. The hidden layer has 10 neurons. Each neuron in one layer is connected with each neuron in the next layer. Each connection has a weight. Each neuron computes the sum of the weighted inputs and the bias. Afterwards, it uses an activation function (e.g. sigmoid function) to compute the output of the neuron and sent the

This article has been accepted for publication in a future issue of this journal, but has not been fully edited. Content may change prior to final publication. Citation information: DOI 10.1109/TPEL.2021.3101713, IEEE Transactions on Power Electronics

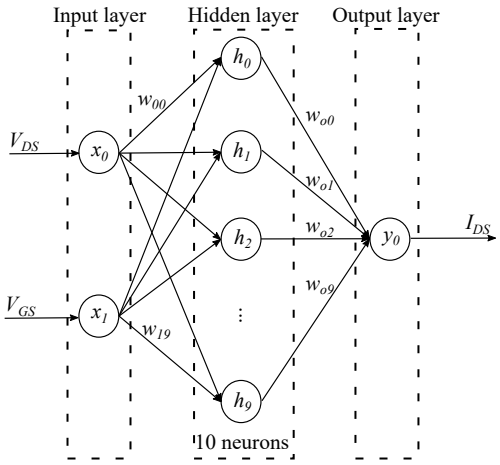

Figure 1. ANN topology.

output to the next layer. The ANN can be represented by the following mathematical equation:

$$I_{DS} = f_{ANN}(V_{DS}, V_{GS}) = \sum_{j=0}^{9}(w_{oj}h_j) + b_o \tag{1}$$
$$= \sum_{j=0}^{9}\left(w_{oj}\left(sigmoid\left(\sum_{i=0}^{1}(w_{ij}x_i) + b_j\right)\right)\right) + b_o.$$

where $\begin{bmatrix} x_0 & x_1 \end{bmatrix} = \begin{bmatrix} V_{DS} & V_{GS} \end{bmatrix}$; w_{oj} is the weight between the j-th hidden-layer neuron and the output neuron; b_o is the bias of the output neuron; h_j is the output of the j-th hidden-layer neuron; b_j is the bias of the j-th hidden-layer neuron; w_{ij} is the weight between the i-th input neuron and the j-th hidden-layer neuron. A sigmoid function is used as the activation function in the hidden layer: $sigmoid\,(x) = \frac{1}{1+e^{-x}}$.

The training process is to tune the weights and biases in the ANN to fit the training data, which are a set of measured characteristics of SiC MOSFETs. A back-propagation algorithm is widely used in the training process [27]. Many software programs have toolboxes to automatically train the ANN, such as the Neural Net Fitting Toolbox in MATLAB.

B. Limitations of the existing ANN model

In the existing ANN model for static simulation [23], the I-V characteristics in a low V_{DS} region are measured by a curve tracer to train the ANN. As shown in Fig. 2a, the ANN model can match the measurement data accurately, which is adequate for static simulation. However, for accurate transient simulation, the model has the following three limitations.

Firstly, the existing ANN model is trained by the I-V characteristics measured in a low V_{DS} region only (0-40 V). However, due to the poor extrapolation ability of the used ANN, the I-V characteristics in the high V_{DS} region from 40 V to the maximum DC voltage ($\geq$ 600 V for CAS120M12BM2) cannot be accurately modeled, which causes inaccurate transient simulation. As shown in Fig. 2b, the existing ANN model has abnormally large saturation current and incorrect off-state current in high V_{DS} region, which are physically wrong for SiC MOSFETs.

Secondly, the off-state, i.e., the cutoff region cannot be accurately modeled. The existing ANN has large errors in the cutoff region as shown in Fig. 2c. There is still significant (even negative) I_{DS} when $V_{DS} = 0\,\text{V}$ or V_{GS} is lower than threshold voltage $V_{GS(th)}$, which is physically wrong according to the physical characteristics of SiC MOSFETs in cutoff region. This is because the ANN is a data-driven model without considering any specific physical characteristics. Also, the training process of ANN is an optimization process to minimize overall error but the local error at a specific region, e.g., cutoff region where I_{DS} is zero, can still be very large.

Thirdly, the C-V characteristics are not considered in the existing ANN model, which are essential for transient simulation. The large variations of C-V characteristics in the whole V_{DS} region must be considered in the modeling method for accuracy.

III. Proposed hybrid modeling methodology for transient simulation

A hybrid modeling methodology is proposed to correspondingly solve the aforementioned three limitations of the existing ANN model described in [23]. The subcircuit model of SiC MOSFETs is presented in Fig. 3. The I-V characteristics of SiC MOSFETs are modeled by the voltage-controlled current source I_{DS} in the subcircuit model. The C-V characteristics are modeled by three variable capacitors C_{GS}, C_{GD}, C_{DS}. Drain-source current I_{DS} and the variable capacitors are modeled as functions of voltages:

$$\begin{cases} I_{DS} &= f_{IV}(V_{DS}, V_{GS}) \\ C_{GS} &= f_{C_{GS}}(V_{DS}) \\ C_{GD} &= f_{C_{GD}}(V_{DS}) \\ C_{DS} &= f_{C_{DS}}(V_{DS}). \end{cases} \tag{2}$$

In this paper, the above functions are modeled by the proposed hybrid data-driven method and then applied in SPICE simulator SIMetrix using Verilog-A language.

A. Data-driven modeling of I-V characteristics in the whole V_{DS} region

The I-V characteristics, including the I_{DS}-V_{DS} characteristics and the I_{DS}-V_{GS} characteristics, were measured by a curve tracer (B1505A; Keysight Technologies, Inc.). The I_{DS}-V_{DS} characteristics measure the drain current I_{DS} by sweeping the drain voltage V_{DS}, while the gate voltage V_{GS} is fixed. The I_{DS}-V_{DS} characteristics can be measured under different gate voltages. In this study, the measurement was performed with V_{DS} between [0, 40] V in steps of 0.8 V and V_{GS} between [0, 20] V in steps of 1 V. The I_{DS}-V_{GS} characteristics measure I_{DS} by sweeping V_{GS}, while V_{DS} is fixed. The I_{DS}-V_{GS} characteristics can be measured under different drain voltages. In this study, the measurement was performed with V_{GS} between [0, 20] V in a step of 0.4 V and V_{DS} between [0, 40] V in a step of 2 V. The circuit to measure the I-V characteristics using the curve tracer B1505A is shown in Fig. 4. It should be noticed that the power supply unit connected to the drain voltage has the output resistance

This article has been accepted for publication in a future issue of this journal, but has not been fully edited. Content may change prior to final publication. Citation information: DOI 10.1109/TPEL.2021.3101713, IEEE Transactions on Power Electronics

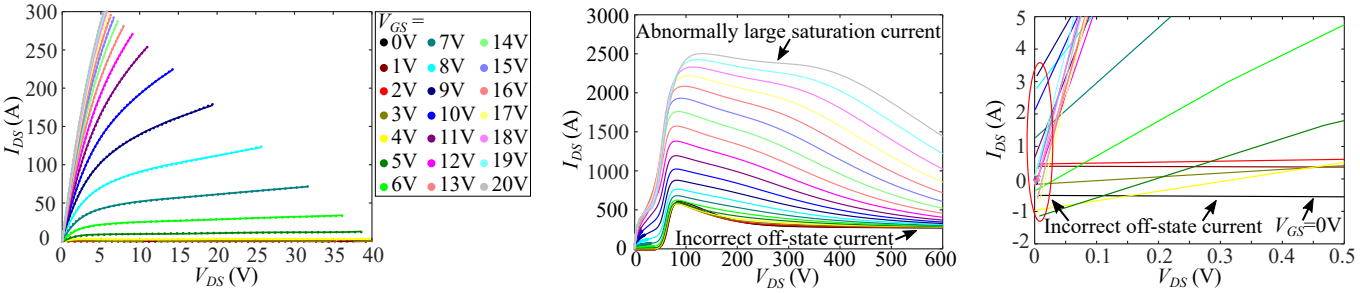

(a) Performance in low V_{DS} region. (b) Performance in whole V_{DS} region. (c) Performance in cutoff region.

Figure 2. Existing ANN model [23] that is trained with measured I-V characteristics in a low V_{DS} region. (Solid lines denote the simulated data. Dots denote the measured data.)

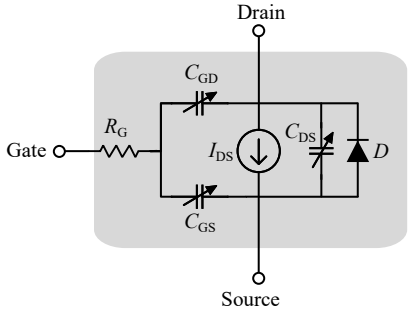

Figure 3. Subcircuit model of SiC MOSFETs.

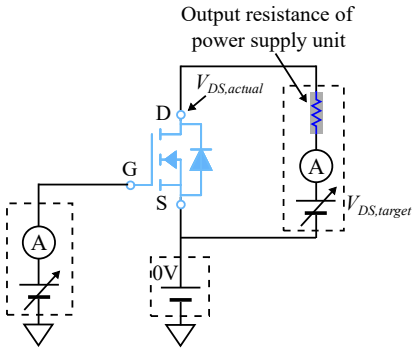

Figure 4. Configuration of the curve tracer B1505A to measure I-V characteristics.

of around 120 mΩ. Due to the voltage drop on this resistance, the actual drain voltage applied to the SiC MOSFET is lower than the targeted drain voltage. Therefore, the actual drain voltage were measured via a Kelvin connection and used in the training data. Due to the limited power rating of the curve tracer and self heating of the device under test, the I-V characteristics can only be measured in the low V_{DS} region ($V_{DS} < 40$ V).

However, the I-V characteristics in the high V_{DS} region (up to the maximum DC voltage across the MOSFETs) have significant impact on the transient simulation [6], [20], [28], [29]. It is shown in Fig. 2b that the existing ANN model cannot simulate the high V_{DS} region correctly. This is caused by the poor extrapolation ability of data-driven-based ANN. The output of ANN is not reliable when the ANN works beyond the region of the training data. The measurement method proposed in [20] was used to measure the I-V characteristics in the

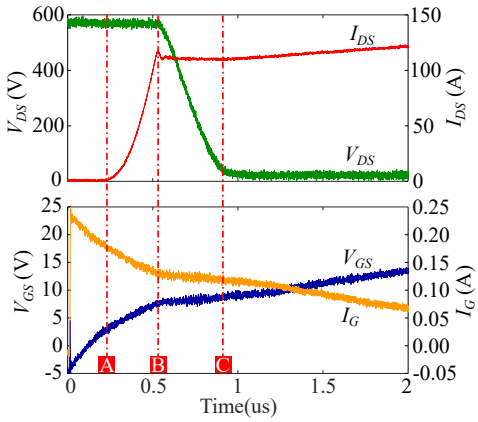

Figure 5. Experiment waveforms of turn-on process to measure the I-V characteristics in the high voltage region.

high V_{DS} region during the turn-on transients. A double pulse tester with a large gate driver resistor (100 Ω) was utilized to slow down the turn-on transients so that the gate plateau can be clearly observed and the effect of parasitic inductance can be ignored. I_{DS} was measured as a function of V_{DS} and V_{GS} at the gate plateau voltage highlighted as Point B in Fig. 5. The turn-on waveforms of I_{DS} and V_{GS} with different turn-on currents under $V_{DC} = 600$ V is shown in Fig. 6. Finally, the I-V characteristics in the high voltage region with $V_{DS} = 50, 100, 200, 300, 400, 500, 600, 700\,V$ and $V_{GS} = 4, 5, 6, 7, 8$ V were used as training data. It is worth mentioning that although the breakdown voltage of the device under test is 1200 V, the I-V characteristics at $V_{DS} = 1200$ V cannot be measured using this method because overshoot voltage during the switching transient might exceed the breakdown voltage and damage the device. In practice, the maximum allowable DC voltage across the device is derated to avoid breakdown. Therefore, the I-V characteristics up to the designed maximum DC voltage were measured. In this paper, the DC source voltage is 600 V. The I-V characteristics up to 700 V were measured and used to train the model considering the voltage overshoot.

The measured I-V characteristics in the whole operation region (i.e., both low and high V_{DS} regions) were used to train the ANN model in Fig. 1. The Neural Net Fitting Toolbox in MATLAB based on backpropagation algorithm was used. The performance of the trained ANN model is shown in Fig. 7. In

This article has been accepted for publication in a future issue of this journal, but has not been fully edited. Content may change prior to final publication. Citation information: DOI 10.1109/TPEL.2021.3101713, IEEE Transactions on Power Electronics

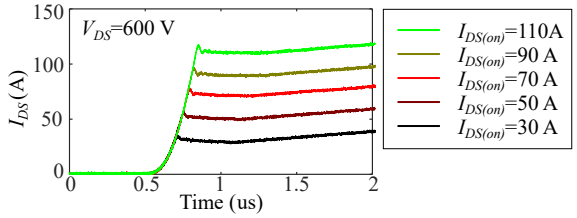

(a) I_{DS}.

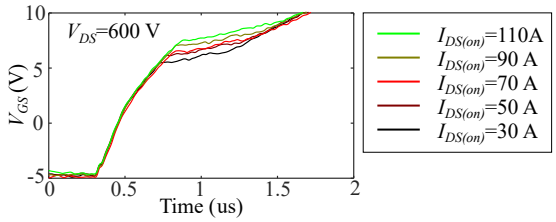

(b) V_{GS}.

Figure 6. Turn-on waveforms of I_{DS} and V_{GS} with different turn-on current under $V_{DC} = 600$ V. (The measured V_{GS} waveform is processed with a 20 MHz low pass filter to eliminate the jitter in the waveform.)

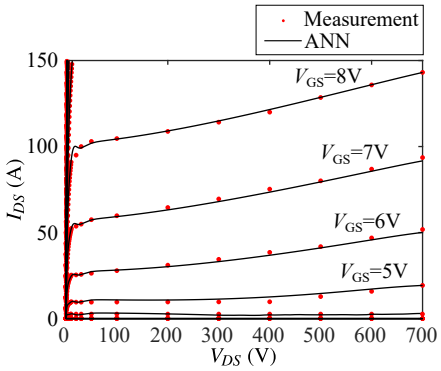

(a) Performance in whole V_{DS} region.

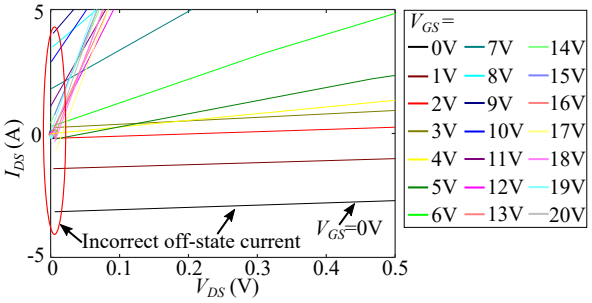

(b) Performance in cutoff region.

Figure 7. ANN model trained with I-V characteristics in whole V_{DS} region. (Solid lines denote the simulated data. Dots denote the measured data.)

Fig. 7a , it can be seen that the trained ANN model can match the I-V characteristics in the whole V_{DS} region. However, the cutoff region still cannot be correctly modeled in Fig. 7b.

B. Hybrid modeling with behavior-based model for cutoff region

As discussed in Section II, the cutoff region cannot be modeled correctly by the ANN shown in Fig. 1. One possible solution is to increase the number of neurons to reduce the errors, but it might cause overfitting problems which will be discussed in Section III-D. Instead of the ANN model which is purely data-driven without considering any physical behaviors, simple equations are very suitable for cutoff region due to the simple physical characteristics in this region. Therefore, we propose a hybrid modeling method that uses equations to model the low-voltage cutoff region and a DPT-data-based ANN to model the high voltage behavior. According to the semiconductor characteristics of SiC MOSFETs, the cutoff region can be divided into two parts:

1) Part I: $V_{GS} < V_{GS(th)}$

When $V_{GS} < V_{GS(th)}$, the drain-to-source current is pinched off since a conductive current channel is not formed due to the insufficient gate-to-source electrical field. To incorporate this physical behavior with the ANN model, a hyperbolic function is used to model the cutoff region when $V_{GS} < V_{GS(th)}$:

$$I_{DS} = f_{ANN}\left(V_{DS}, V_{GS}\right) \cdot f_{cutoff}\left(V_{GS}\right). \tag{3}$$

$$f_{cutoff}\left(V_{GS}\right) = \frac{1}{2}\left(1 + \tanh\left(\alpha\left(V_{GS} - V_{GS(th)}\right)\right)\right). \tag{4}$$

The threshold voltage can be measured by a curve tracer. The hyperbolic function is used to keep the model continuous. α is set large enough ($\alpha = 10$) to make sure that $I_{DS} \approx 0$ when $V_{GS} < V_{GS(th)}$ and $I_{DS} \approx f_{ANN}\left(V_{DS}, V_{GS}\right)$ when $V_{GS} > V_{GS(th)}$.

2) Part II: $V_{DS} = 0\,\mathrm{V}$

I_{DS} should be zero when $V_{DS} = 0\,\mathrm{V}$. To model this physical behavior, the linear region where V_{DS} is close to $0\,\mathrm{V}$ is modeled together. According to the physical characteristics of SiC MOSFETs, when $V_{GS} > V_{GS(th)}$ and V_{DS} is smaller than the saturation voltage V_{sat}, the MOSFET operates like a resistor controlled by V_{GS}. Therefore, the linear region can be modeled by the following proportional function:

$$I_{DS} = \frac{f_{ANN}\left(V_{sat}, V_{GS}\right)}{V_{sat}} \cdot V_{DS} \quad \text{if } 0 \le V_{DS} < V_{sat}. \tag{5}$$

For the selected power module CAS120M12BM2, the linear region is $0\,\mathrm{V} \leqslant V_{DS} \leqslant 2\,\mathrm{V}$. Therefore, $V_{sat} = 2\,\mathrm{V}$ is selected. This equation is valid in the linear region of the SiC MOSFET and it can also guarantee that the SiC MOSFET is cut off when $V_{DS} = 0\,\mathrm{V}$. $f_{ANN}\left(V_{sat}, V_{GS}\right)/V_{sat}$ is used as the slope of the proportional equation to keep it continuous with the ANN model for convergence of the whole model.

Finally, the hybrid data-driven model for I-V characteristics can be built by combining (4) and (5) with the ANN model in (1). The hybrid model is written as follows:

$$I_{DS} = \begin{cases} f_{ANN}\left(V_{DS}, V_{GS}\right) \cdot f_{cutoff}\left(V_{GS}\right), \\ \qquad\qquad \text{if } V_{DS} \ge V_{sat}, \\ f_{ANN}\left(V_{sat}, V_{GS}\right) \cdot \frac{V_{DS}}{V_{sat}} \cdot f_{cutoff}\left(V_{GS}\right), \\ \qquad\qquad \text{if } 0\,\mathrm{V} \le V_{DS} < V_{sat}. \end{cases} \tag{6}$$

As shown in Fig. 8a, the I-V characteristics where $0\,V \le V_{DS} < V_{sat}$ or $V_{GS} < V_{GS(th)}$, i.e., the region in purple, is modeled by behavior-based model. The remaining part, i.e., the region in gray, is modeled by data-driven ANN model. As shown in Fig. 8, the I-V characteristics in the whole V_{DS} region and cutoff region can be accurately modeled by the proposed hybrid modeling method.

This article has been accepted for publication in a future issue of this journal, but has not been fully edited. Content may change prior to final publication. Citation information: DOI 10.1109/TPEL.2021.3101713, IEEE Transactions on Power Electronics

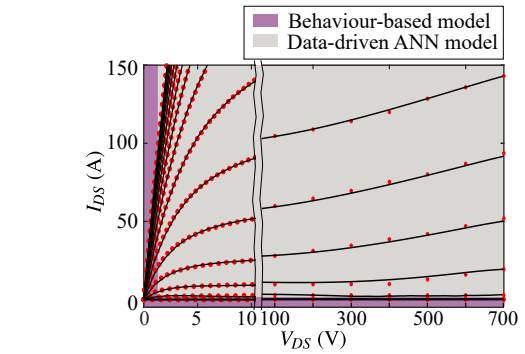

(a) Hybrid I_{DS} model.

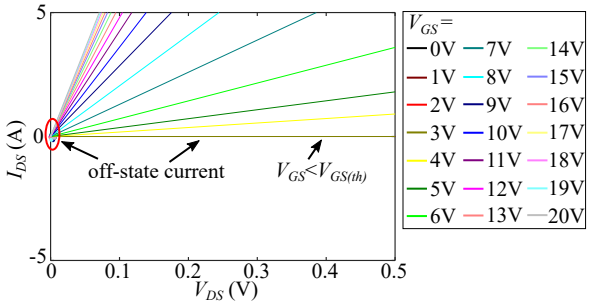

(b) Performance in cutoff region.

Figure 8. Performance of the proposed hybrid modeling methodology.

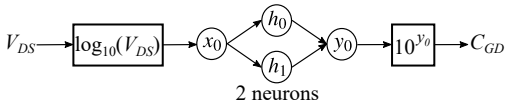

(a) C_{GD} model.

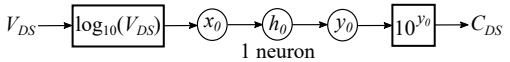

(b) C_{DS} model.

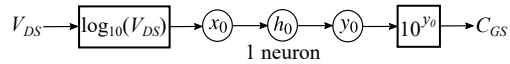

(c) C_{GS} model.

Figure 9. ANN capacitance models trained in logarithmic scale.

C. Modeling of C-V characteristics

C-V characteristics are essential for transient simulation [30], which were built with ANNs in this study for accuracy and adaptability. It is worth noting that the measured C_{GD} reduces by almost 20 times from 2600 pF to 150 pF when V_{DS} changes from 0 V to 20 V but has only minor variations when $V_{DS} > 20$ V. The characteristics of C_{DS} are similar. Therefore, for model accuracy, the training data were measured in logarithmic scale and the logarithmic transformation is adopted in the ANN models to balance large data variations. The ANN models with logarithmic transformation are shown in Fig. 9. The number of neurons in the hidden layer to model C_{GD}, C_{GS} and C_{DS} are 2, 1 and 1 respectively. The C-V characteristics were measured using the curve tracer B1505A. The input capacitance C_{iss}, output capacitance C_{oss} and reverse transfer capacitance C_{rss} were measured as a function of V_{DS} from 0.01 V to 1000 V in logarithmic scale with 251 data points. The gate-to-source capacitance C_{GS}, gate-to-drain capacitance C_{GD} and drain-to-source capacitance C_{DS} can be calculated accordingly:

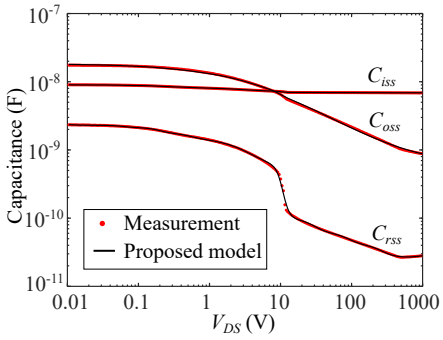

Figure 10. Results of ANN capacitance models trained in logarithmic scale.

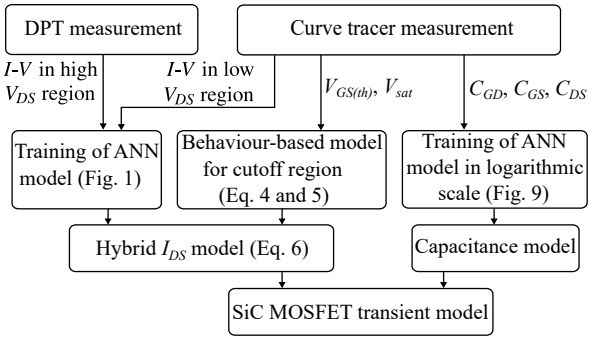

Figure 11. Flowchart of the proposed hybrid modeling methodology.

$$\begin{cases} C_{GD} &= C_{rss} \\ C_{GS} &= C_{iss} - C_{rss} \\ C_{DS} &= C_{oss} - C_{rss}. \end{cases} \tag{7}$$

The calculated C_{GD}, C_{GS} and C_{DS} were used as training data to train the ANN models. As shown in Fig. 10, the ANN models can simulate the capacitance characteristics accurately.

D. Modeling flowchart and neural network selection

The flowchart of the proposed modeling methodology is summarized in Fig. 11. The I-V characteristics were measured by curve tracer and DPT to train the ANN model. Behavior-based model for cutoff region was built with measured $V_{GS(th)}$ and V_{sat}. The hybrid I_{DS} model was built by combining the behavior-based model with ANN model. C-V characteristics were measured to train the ANN models of C_{GD}, C_{DS} and C_{GS} in logarithmic scale.

For the neural network selection, there is no exact standard to follow to determine the number of layers and neurons of the ANN for a certain application [23]. In this study, it is shown that ANNs with single hidden layer are sufficient to model the nonlinear I-V and C-V characteristics of SiC MOSFETs. The analytical formulas of single-hidden-layer ANNs can also be obtained straightforwardly. ANNs with more than one hidden layer can also be used, but the analytical formulas become more complex. The investigation of ANN models with different number of hidden layers is beyond the scope of this paper.

This article has been accepted for publication in a future issue of this journal, but has not been fully edited. Content may change prior to final publication. Citation information: DOI 10.1109/TPEL.2021.3101713, IEEE Transactions on Power Electronics

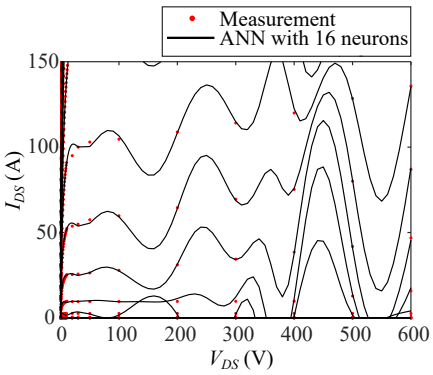

Figure 12. Overfitting of ANN with excessive hidden neurons.

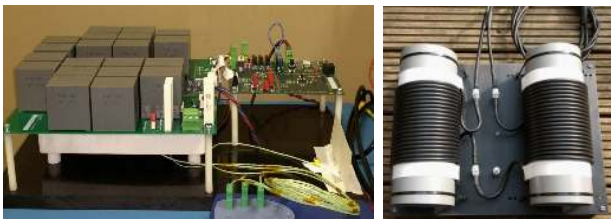

(a) Double pulse tester. (b) Load inductor.

Figure 13. Experimental setup.

After the single-hidden-layer ANN was selected, the number of neurons in the hidden layer should be chosen. The trial-and-error method was used, which was achieved by training ANNs with different number of neurons and selecting the minimum number of neurons that can provide accurate approximation. Although using more neurons can help reduce the training errors of ANNs, it will increase the computation time and might cause overfitting problems of ANNs [31]. The overfitting phenomenon of the ANN with 16 hidden neurons to model the I-V characteristics is shown in Fig. 12. It can be seen that the ANN has unexpected output current, although the measurement data of I-V characteristics can be matched accurately. In this paper, single-hidden-layer ANN with 10 neurons was selected to model the I-V characteristics. ANNs with 2, 1 and 1 neurons were selected to model C_{GD}, C_{GS} and C_{DS} of a SiC MOSFET module, respectively. It is expected that a similar number of neurons is enough to model any SiC MOSFETs as they have similar shapes of I-V and C-V characteristics, although voltage and current levels are distinct.

Note that temperature characteristics of SiC MOSFETs are not considered here. The I-V characteristics, C-V characteristics and the switching transients of SiC MOSFETs were all measured at 25 °C. The temperature characteristics can be easily added into the model through adding a third input node to the ANN model in Fig. 1 and then training the model with temperature-dependent I-V data, which can be measured using a curve tracer and DPT.

IV. Experimental Model Verification

In this section, the simulated and experimental waveforms of the switching transients of SiC MOSFETs were compared using a double-pulse tester (DPT) to verify the proposed modeling method. To demonstrate the repeatability of the proposed modeling method, two samples of 1200 V SiC half-bridge modules from Wolfspeed, i.e., CAS120M12BM2, were used to facilitate the verification. One sample was used to measure the training dataset. The training dataset was then used to train the ANN-based model. After the model was trained, the switching transients of SiC MOSFETs were simulated and compared with the switching waveforms measured from another sample.

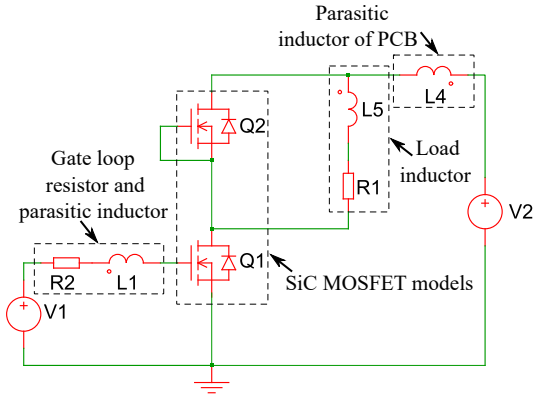

Figure 14. Simulation circuit of DPT in SIMetrix.

The proposed modeling method can be adopted in widely-used simulation tools such as SPICE simulators. A transient model of the power module CAS120M12BM2 was built based on the proposed hybrid modeling method. It was then implemented in SIMetrix using Verilog-A language. Verilog-A is a widely-used modeling language for analog circuits, which can be used in a SPICE environment [32]. It is flexible with user defined functions and variable data types like arrays [33]. As a result, the matrix-based analytical equations in the trained ANN and cut-off region models can be easily implemented using Verilog-A. The anti-parallel diode model in [7] and the stray inductance of CAS120M12BM2 in [34] were used in the model. The internal gate resistor is 1.8 Ω measured using the Keysight curve tracer B1505A. Experiment and simulation platforms of DPT were built to verify the proposed modeling method for transient simulation.

In the experimental platform shown in Fig. 13a, a DPT with low stray inductance was designed for the half-bridge module CAS120M12BM2. A commercial gate driver CGD15HB62P1 for half-bridge module from Wolfspeed was used. Two air-core inductors were designed and connected in series as the load inductor as shown in Fig. 13b. For this inductor, the total inductance is 55.7 μH with equivalent series resistance of 0.064 Ω and equivalent parallel capacitance of 140 pF.

The DPT circuitry was simulated using SPICE simulator SIMetrix as shown in Fig 14. Q_1 and Q_2 are the proposed SiC MOSFET models. The DC-bus stray inductance was obtained by simulating the S-parameter of the PCB board in Keysight Advanced Design System. The proposed model was simulated and then compared with the experimental results from DPT. As shown in Fig. 15, the simulated turn-on and turn-off waveforms of the proposed model can match the experimental results accurately. The turn-on/off delay time $T_{d(on)}$ and $T_{d(off)}$, rise/fall time T_r and T_f, turn-on/off losses E_{on} and E_{off} of the proposed model were calculated according to the IEC 60747-8 definitions and compared with experimental results in Table I. It is shown that the errors of the proposed model are all within 11%.

This article has been accepted for publication in a future issue of this journal, but has not been fully edited. Content may change prior to final publication. Citation information: DOI 10.1109/TPEL.2021.3101713, IEEE Transactions on Power Electronics

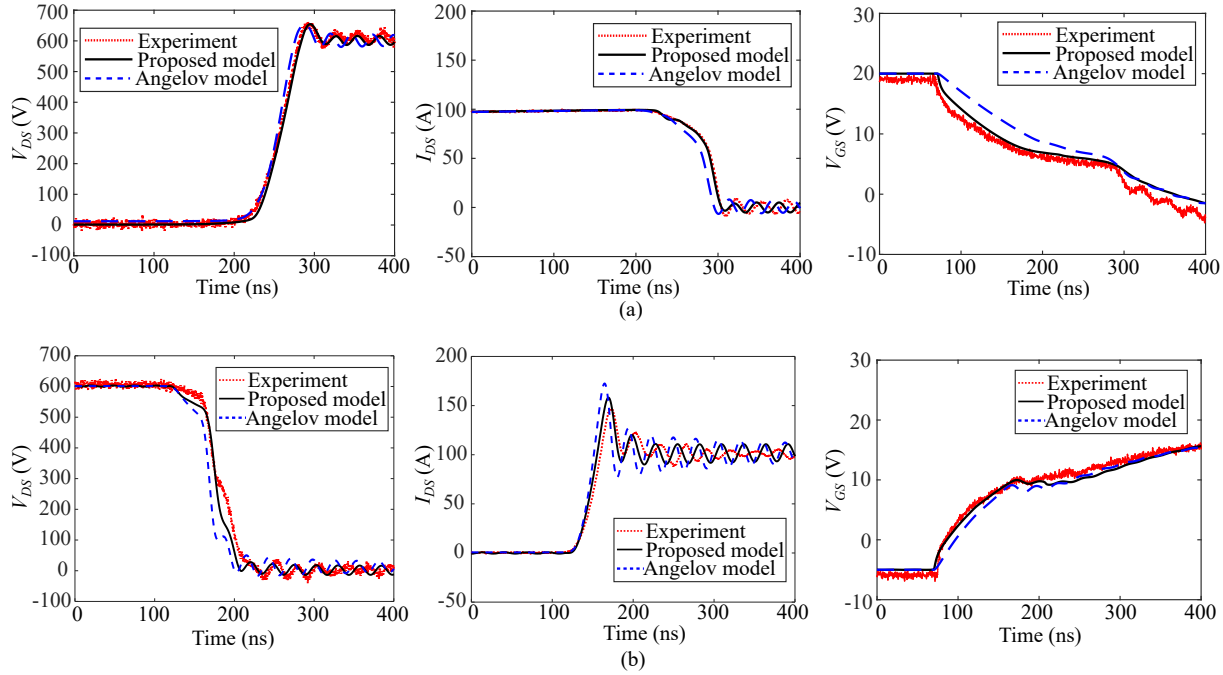

Figure 15. Measured and simulated (a) turn-off and (b) turn-on transients.

Table I
COMPARISON RESULTS OF SWITCHING TRANSIENTS.

Test conditions	Experiment	Proposed model	Errors of proposed model	Angelov model	Errors of Angelov model
Turn on	$T_{d(on)}$ = 87.6 ns	$T_{d(on)}$ = 78.6 ns	10.27%	$T_{d(on)}$ =57.1 ns	34.82%
	T_r = 44.0 ns	T_r = 48.7 ns	10.68%	T_r = 53.0 ns	20.45%
	E_{on} =2.649 mJ	E_{on} =2.818 mJ	6.39%	E_{on} =2.072 mJ	21.78%
Turn off	$T_{d(off)}$ = 155.5 ns	$T_{d(off)}$ = 156.1 ns	0.39%	$T_{d(off)}$ =126.3 ns	18.78%
	T_f = 46.3 ns	T_f = 45.2 ns	2.38%	T_f = 43.5 ns	6.05%
	E_{off} =1.556 mJ	E_{off} =1.637 mJ	5.21%	E_{off} = 1.738 mJ	11.70%

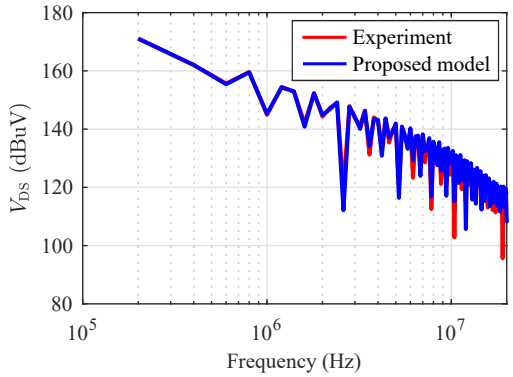

Figure 16. Comparison of Drain-Source voltage spectra of experimental and simulation results.

To conduct the EMI analysis, the EM noise induced by the switching transients needs to be calculated in frequency domain [9]. For this purpose, the simulated and experimental switching waveforms of the Drain-Source voltage presented in Fig. 15 were used for spectrum analysis. The spectra of the experimental and simulated Drain-Source voltage waveforms were computed via fast Fourier transformation in MATLAB. The comparison of the Drain-Source voltage spectra is shown in Fig. 16. The red line represents the spectrum of experimental result, and the blue one represents the spectrum of the simulation result derived from the proposed model. It is found that the simulated spectrum by the proposed model matches well with the experimentally obtained spectrum. The relative RMS error of the simulated spectrum extracted using the proposed model is 2.82%, which is calculated according to (8).

V. COMPARISONS WITH ANGELOV MODEL

In this section, the proposed hybrid data-driven model was compared with the commercial Angelov model proposed in [20] to further demonstrate the accuracy and speed of the proposed model. The Angelov model was selected for comparison because it is a standard industry behavior model from Keysight to simulate transient waveforms of SiC MOSFETs accurately [28]. To facilitate the comparison, the same measured data were used to build the proposed model and the Angelov model. The parameters of the Angelov model was extracted in IC-CAP. Although the parameters of Angelov model can be automatically extracted in IC-CAP by fitting the simulated data to the measured data, the accuracy of the fitting results

This article has been accepted for publication in a future issue of this journal, but has not been fully edited. Content may change prior to final publication. Citation information: DOI 10.1109/TPEL.2021.3101713, IEEE Transactions on Power Electronics

Table II
RELATIVE RMS ERRORS OF SWITCHING TRANSIENTS.

Test conditions	Transient waveforms	Proposed model	Angelov model
Turn off	V_{DS}	3.84%	5.96%
	I_{DS}	3.82%	12.07%
	V_{GS}	12.07%	35.24%
Turn on	V_{DS}	6.33%	13.76%
	I_{DS}	10.78%	20.80%
	V_{GS}	7.83%	11.85%

Table III
RELATIVE RMS ERRORS OF C-V AND I-V CHARACTERISTICS.

	C_{iss}	C_{oss}	C_{rss}	I_{DS}
Proposed model	0.37%	1.7%	1.8%	2.81%
Angelov model	1.31%	4.99%	10.02%	9.63%

was not satisfactory. The parameters still need to be tuned manually to achieve the required accuracy. Afterwards, the Angelov model is used as Q_1 and Q_2 in Fig. 14 to simulate the switching transient waveforms in a DPT circuit.

A. Model accuracy

The transient simulations of both models are compared in Fig. 15, against experimental results from DPT. It can be seen that the proposed model is more accurate than the Angelov model comparing to the experimental turn-on/off waveforms. The turn-on/off delay time $T_{d(on)}$ and $T_{d(off)}$, rise/fall time T_r and T_f, turn-on/off losses E_{on} and E_{off} of both models were calculated and compared with experimental results in Table I. The comparison shows that the proposed model has smaller errors than Angelov model. The errors of the proposed model are reduced by at least two times comparing to the Angelov model.

The relative root-mean-square (RMS) error were used to quantitatively compare the accuracy of switching waveforms of these two models. The relative RMS Error can be calculated as follows:

$$\text{Relative RMS Error} = \sqrt{\frac{\sum_{i=1}^{N} |m_i - s_i|^2}{\sum_{i=1}^{N} |m_i|^2}} \times 100\%. \quad (8)$$

where m_i and s_i denote the measured and simulated values (V_{DS}, V_{GS} and I_{DS} in Fig. 15) at the i-th data point, respectively; N denotes the total number of data points.

The calculated relative RMS errors of the simulated switching waveforms in Fig. 15 are shown in Table II. The relative RMS errors of the proposed model are $1.5 \sim 3$ times smaller than those of the Angelov model.

In Fig. 16, the relative RMS error of the simulated Drain-Source voltage spectrum obtained via the proposed model is 2.82%. As a comparison, the RMS error of the simulated spectrum obtained via the Angelov model is 4.26%, which is about 1.5 times higher compared to the proposed model.

Although both models were built with the same measured I-V and C-V characteristics, the proposed model is more accurate than the Angelov model in transient simulation. This is because the proposed model can match the measured I-V and C-V data more accurately than the Angelov model. The simulated I-V and C-V characteristics of the proposed model and Angelov model were compared with the measured characteristics in Fig. 17 and Fig. 18, which show that the proposed model can match the measured data more accurately than the Angelov model.

The relative RMS errors of the C-V and I-V characteristics of the proposed model and Angelov model are calculated according to Fig. 17 and Fig. 18 and the results are shown in Table III. The relative RMS errors of the proposed model are much smaller than those of the Angelov model. Consequently, the proposed model can provide more accurate transient simulation results for switching losses and EMI analysis.

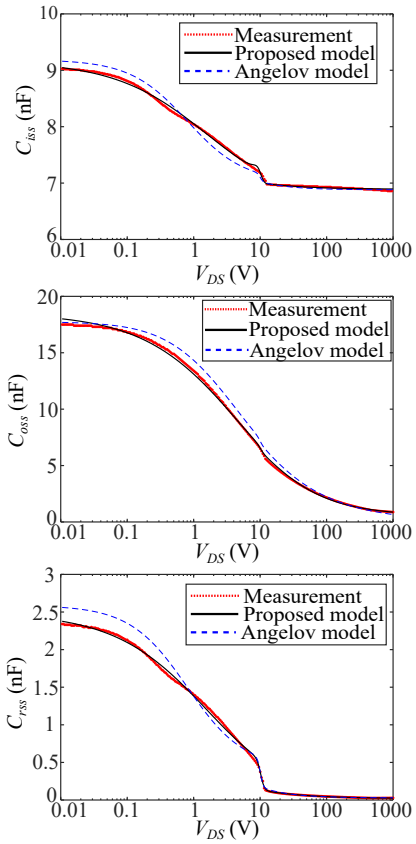

Figure 17. Comparison of C-V characteristics of proposed model and Angelov model.

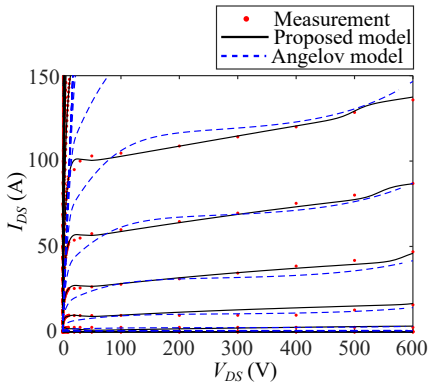

Figure 18. Comparison of I-V characteristics of proposed model and Angelov model.

This article has been accepted for publication in a future issue of this journal, but has not been fully edited. Content may change prior to final publication. Citation information: DOI 10.1109/TPEL.2021.3101713, IEEE Transactions on Power Electronics

Table IV
COMPARISON OF COMPUTATION TIME BETWEEN THE PROPOSED MODEL AND ANGELOV MODEL.

	Proposed model	Angelov model
Simulation runtime (s)	3.13	4.46

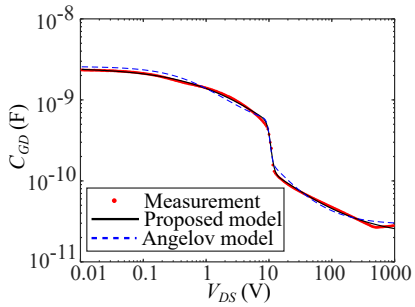

(a) CAS120M12BM2 from Wolfspeed.

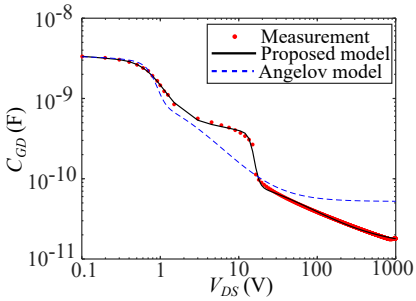

(b) MSC025SMA120S from Microsemi.

Figure 19. Simulated and measured C_{GD} characteristics of two different devices.

B. Computation time

The computation time of the proposed model was compared with the Angelov model through simulating the same DPT circuit in SIMetrix for 40 μs. The runtime of the simulations was recorded, which was directly captured by SIMetrix. For accuracy, the simulation of each model was repeated 20 times in SIMetrix and the average runtime was used. The computer configuration used for the comparison is: Intel Core i7-8650U CPU@1.9GHz, 16-GB RAM. The version of SIMetrix is 8.00g and the default solver parameters of SIMetrix were used. It is shown in Table IV that the runtime of the proposed model when simulating the DPT circuit is about 30% less compared to the Angelov model.

C. Model adaptability

SiC MOSFETs from different manufacturers might have different device characteristics due to technology differences. Although both the proposed model and Angelov model can be used to model different SiC MOSFETs, the parameters of both models must be adjusted according to the characteristics of each MOSFET. For the proposed model, the weights and biases of the ANNs are trained by different device characteristics according to the flowchart in Fig. 11. For the Angelov model, the parameters are extracted based on the curve fitting method to match specific device characteristics.

In Fig. 19, the C_{GD} characteristics of two SiC MOSFETs were measured and modeled by the proposed model and the Angelov model. The first device is CAS120M12BM2 from Wolfspeed and the second one is MSC025SMA120S from Microsemi. It is shown that these two devices have different C_{GD} characteristics. As the conventional behavior model, the Angelov model can well match the C_{GD} characteristics of CAS120M12BM2, but it failed to accurately match the C_{GD} characteristics of MSC025SMA120S. The proposed ANN-based model has much better adaptability comparing to the Angelov model. The different C_{GD} characteristics of both devices can be simulated accurately by the proposed model.

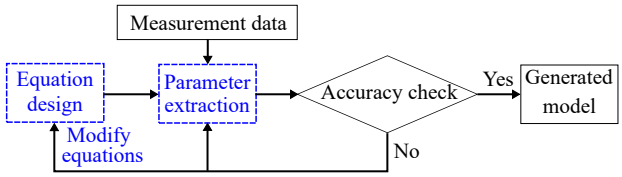

(a) Angelov model.

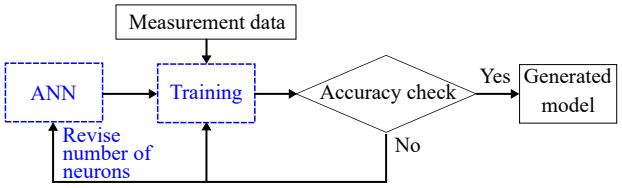

(b) Proposed ANN-based model.

Figure 20. Modeling processes of Angelov and proposed ANN-based model.

D. Modeling process

Both Angelov and the proposed ANN-based models are parameter based models. Parameters of the proposed model are more difficult to be manually altered because there are no clear relationship between the ANN parameters and the model behavior. However, thanks to the well-developed Neural Net Fitting Toolbox in MATLAB, the parameters of the ANN-based model can be trained automatically. The general modeling processes of the Angelov model and the proposed ANN-based model are shown in Fig. 20. The difference between the modeling processes of two models is highlighted in blue dashed blocks.

For the Angelov model, the mathematical equations are firstly designed according to the device characteristics. Afterwards, the parameters of the equations are extracted. If the parameter extraction results are not accurate enough after the manual tuning, the equations in the original Angelov model need to be modified and the parameters need to be extracted again. As a result, there is potentially a lot of manual work, which is time-consuming and requires expert experience.

On the other hand, for the proposed ANN-based model, the single-hidden-layer ANN is used so there is no need to design complicated equations. The training of ANN is fully automatic based on Neural Net Fitting Toolbox in MATLAB. If the training results are not accurate enough, the ANN model can be modified by simply revising the number of neurons in the hidden layer and the modified model can be trained quickly. Comparing to the conventional modeling process, the ANN-based modeling process requires less manual work so is more time-efficient.

VI. Conclusion

In this paper, a hybrid data-driven modeling methodology has been proposed to model SiC MOSFETs for accurate and fast transient simulation. To accurately model the high-speed switching transients, the required training dataset were identified and then measured to train the proposed ANN model. The trained ANN was combined with the behavior-based equations to accurately model the cut-off region and to avoid overfitting the ANN model. In addition, the C-V characteristics were modeled in logarithmic scale using ANNs for accuracy. The accuracy and repeatability of the proposed modeling method have been verified through modeling and testing two SiC MOSFET module samples of CAS120M12BM2. One sample was used to measure the training dataset and the other sample to perform experimental verification. The simulated transient waveforms were compared with the experimental turn on/off waveforms from a DPT to demonstrate the accuracy of the proposed modeling methodology.

To further demonstrate the accuracy and speed of the proposed model, it has been compared with the Angelov model in detail. The switching transients of the proposed model are $1.5 \sim 3$ times closer to the experimental results compared to the Angelov model. The runtime of both models was compared through simulating the same DPT circuit in SPICE simulator SIMetrix. The simulation runtime of the proposed hybrid model is found to be 30% reduced compared to the Angelov model. Besides, the proposed hybrid data-driven modeling method has better adaptability to model devices from different manufactures and the modeling process of the proposed method is more convenient and time-efficient.

References

[1] S. Hazra *et al.*, "High switching performance of 1700-V, 50-A SiC power MOSFET over Si IGBT/BiMOSFET for advanced power conversion applications," *IEEE Trans. Power Electron.*, vol. 31, no. 7, pp. 4742–4754, 2016.

[2] K. Hamada, M. Nagao, M. Ajioka, and F. Kawai, "SiC-Emerging power device technology for next-generation electrically powered environmentally friendly vehicles," *IEEE Trans. Electron Devices*, vol. 62, no. 2, pp. 278–285, 2015.

[3] B. Cougo, H. H. Sathler, R. Riva, V. D. Santos, N. Roux, and B. Sareni, "Characterization of low-inductance SiC module with integrated capacitors for aircraft applications requiring low losses and low EMI issues," *IEEE Trans. Power Electron.*, vol. 36, no. 7, pp. 8230–8242, 2021.

[4] H. Zhao *et al.*, "Physics-based modeling of parasitic capacitance in medium-voltage filter inductors," *IEEE Trans. Power Electron.*, vol. 36, no. 1, pp. 829–843, 2021.

[5] N. Oswald, P. Anthony, N. McNeill, and B. H. Stark, "An experimental investigation of the tradeoff between switching losses and EMI generation with hard-switched all-Si, Si-SiC, and all-SiC device combinations," *IEEE Trans. Power Electron.*, vol. 29, no. 5, pp. 2393–2407, 2014.

[6] Y. Mukunoki *et al.*, "An improved compact model for a Silicon-Carbide MOSFET and its application to accurate circuit simulation," *IEEE Trans. Power Electron.*, vol. 33, no. 11, pp. 9834–9842, 2018.

[7] S. Yin *et al.*, "An accurate subcircuit model of SiC half-bridge module for switching-loss optimization," *IEEE Trans. Ind. Appl.*, vol. 53, no. 4, pp. 3840–3848, 2017.

[8] Z. Zeng, X. Zhang, F. Blaabjerg, H. Chen, and T. Sun, "Stepwise design methodology and heterogeneous integration routine of air-cooled SiC inverter for electric vehicle," *IEEE Trans. Power Electron.*, vol. 35, no. 4, pp. 3973–3988, 2020.

[9] Y. Wu, S. Yin, H. Li, and W. Ma, "Impact of RC snubber on switching oscillation damping of SiC MOSFET with analytical model," *IEEE Trans. Emerg. Sel. Topics Power Electron.*, vol. 8, no. 1, pp. 163–178, 2020.

[10] H. A. Mantooth, K. Peng, E. Santi, and J. L. Hudgins, "Modeling of wide bandgap power semiconductor devices—Part I," *IEEE Trans. Electron Devices*, vol. 62, no. 2, pp. 423–433, 2015.

[11] R. Fu, A. Grekov, J. Hudgins, A. Mantooth, and E. Santi, "Power SiC DMOSFET model accounting for nonuniform current distribution in JFET region," *IEEE Trans. Ind. Appl.*, vol. 48, no. 1, pp. 181–190, 2012.

[12] S. K. Powell, N. Goldsman, J. M. McGarrity, J. Bernstein, C. J. Scozzie, and A. Lelis, "Physics-based numerical modeling and characterization of 6H-silicon-carbide metal–oxide–semiconductor field-effect transistors," *J. Appl. Phys.*, vol. 92, no. 7, pp. 4053–4061, 2002.

[13] V. Talesara *et al.*, "Dynamic switching of SiC power MOSFETs based on analytical subcircuit model," *IEEE Trans. Power Electron.*, vol. 35, no. 9, pp. 9680–9689, 2020.

[14] C. He *et al.*, "A physically based scalable SPICE model for silicon carbide power MOSFETs," in *Proc. IEEE Appl. Power Electron. Conf. Expo.*, 2017, pp. 2678–2684.

[15] Y. Xu, C. Ho, A. Ghosh, and D. Muthumuni, "Design, implementation, and validation of electro-thermal simulation for SiC MOSFETs in power electronic systems," *IEEE Trans. Ind. Appl.*, pp. 1–1, 2021.

[16] K. Han, B. J. Baliga, and W. Sung, "Split-gate 1.2-kV 4H-SiC MOSFET: Analysis and experimental validation," *IEEE Electron Device Lett.*, vol. 38, no. 10, pp. 1437–1440, 2017.

[17] Z. Duan, T. Fan, X. Wen, and D. Zhang, "Improved SiC power MOSFET model considering nonlinear junction capacitances," *IEEE Trans. Power Electron.*, vol. 33, no. 3, pp. 2509–2517, 2018.

[18] A. Rashid, M. M. Hossain, A. Emon, and H. E. C. A. Mantooth, "Datasheet-driven compact model of silicon carbide power MOSFET including third quadrant behavior," *IEEE Trans. Power Electron.*, pp. 1–1, 2021.

[19] H. Li, X. Zhao, K. Sun, Z. Zhao, G. Cao, and T. Zheng, "A non-segmented PSpice model of SiC MOSFET with temperature-dependent parameters," *IEEE Trans. Power Electron.*, vol. 34, no. 5, pp. 4603–4612, 2019.

[20] H. Sakairi, T. Yanagi, H. Otake, N. Kuroda, and H. Tanigawa, "Measurement methodology for accurate modeling of SiC MOSFET switching behavior over wide voltage and current ranges," *IEEE Trans. Power Electron.*, vol. 33, no. 9, pp. 7314–7325, 2018.

[21] W. Jouha, A. E. Oualkadi, P. Dherbécourt, E. Joubert, and M. Masmoudi, "Silicon carbide power MOSFET model: An accurate parameter extraction method based on the levenberg-marquardt algorithm," *IEEE Trans. Power Electron.*, vol. 33, no. 11, pp. 9130–9133, 2018.

[22] Keysight Technologies, Angelov model. [Online]. Available: https://edadocs.software.keysight.com/pages/viewpage.action?pageId=5692701

[23] D. Chiozzi, M. Bernardoni, N. Delmonte, and P. Cova, "A neural network based approach to simulate electrothermal device interaction in SPICE environment," *IEEE Trans. Power Electron.*, vol. 34, no. 5, pp. 4703–4710, 2019.

[24] S. Hatami, M. Azizi, H. Bahrami, D. Motavalizadeh, and A. Afzali-Kusha, "Accurate and efficient modeling of SOI MOSFET with technology independent neural networks," *IEEE Trans. Comput.-Aided Design Integr. Circuits Syst.*, vol. 23, no. 11, pp. 1580–1587, 2004.

[25] H. B. Hammouda, M. Mhiri, Z. Gafsi, and K. Besbes, "Neural-based models of semiconductor devices for SPICE simulator," *Am. J. Appl. Sci.*, vol. 5, no. 4, pp. 385–391, 2008.

[26] G. Cybenko, "Approximations by superpositions of a sigmoidal function," *Math. of Con.l, Signals, and Syst.*, vol. 2, pp. 183–192, 1989.

[27] G. F. Luger, *Artificial intelligence: structures and strategies for complex problem solving*. Pearson education, 2005.

[28] Y. Nakamura, N. Kuroda, T. Yanagi, H. Sakairi, and K. Nakahara, "High-voltage and high-current Id-Vds measurement method for power transistors improved by reducing self-heating," *IEEE Electron Device Lett.*, vol. 41, no. 4, pp. 581–584, 2020.

[29] Z. Dong, X. Wu, H. Xu, N. Ren, and K. Sheng, "Accurate analytical switching-on loss model of SiC MOSFET considering dynamic transfer characteristic and Qgd," *IEEE Trans. Power Electron.*, vol. 35, no. 11, pp. 12 264–12 273, 2020.

[30] K. Chen, Z. Zhao, L. Yuan, T. Lu, and F. He, "The impact of nonlinear junction capacitance on switching transient and its modeling for SiC MOSFET," *IEEE Trans. Electron Devices*, vol. 62, no. 2, pp. 333–338, 2015.

[31] Y. Liu, J. A. Starzyk, and Z. Zhu, "Optimized approximation algorithm in neural networks without overfitting," *IEEE Trans. Neural Netw.*, vol. 19, no. 6, pp. 983–995, 2008.

[32] C. C. McAndrew, "SPICE modeling in verilog-A: Successes and challenges: Invited paper," in *Proc. 47th Eur. Solid-State Device Res. Conf. (ESSDERC)*, 2017, pp. 22–25.

[33] F. García-Redondo, R. P. Gowers, A. Crespo-Yepes, M. López-Vallejo, and L. Jiang, "SPICE compact modeling of bipolar/unipolar memristor switching governed by electrical thresholds," *IEEE Trans. Circuits Syst. I, Reg. Papers*, vol. 63, no. 8, pp. 1255–1264, 2016.

[34] Y. Liu, K. Y. See, S. Yin, R. Simanjorang, A. K. Gupta, and J. Lai, "Equivalent circuit model of high power density SiC converter for common-mode conducted emission prediction and analysis," *IEEE Electromagn. Compat. Mag.*, vol. 8, no. 1, pp. 67–74, 2019.

Peng Yang (M'16) received the B.Sc and M.Sc degrees in electrical engineering from Tsinghua University, Beijing, China, in 2015 and 2018, respectively. From 2018 to 2021, he was a Marie Curie Early Stage Research Fellow funded by the European Union's InnoDC project. He is currently working toward the Ph.D. degree in electrical engineering at Cardiff University, UK. His research interests focus on characterization, modeling and applications of wide bandgap semiconductors in power electronics.

Wenlong Ming (M'16) received the B.Eng. and M.Eng. Degrees in Automation from Shandong University, Jinan, China, in 2007 and 2010, respectively. He received the Ph.D. degree in Automatic Control and Systems Engineering from the University of Sheffield, Sheffield, U.K., in 2015. He is the winner of the prestigious IET Control & Automation Doctoral Dissertation Prize in 2017. He has been a Senior Lecturer of Power Electronics at Cardiff University, U.K., since August 2020 and a Senior Research Fellow funded by Compound Semiconductor Applications (CSA) Catapult, U.K., for 5 years since April 2020.

He was with the Center for Power Electronics Systems (CPES), Virginia Tech, Blacksburg, USA in 2012 as an academic visiting scholar. He has (co-)authored more than 60 papers published in leading journals or refereed IEEE conferences. His research interests focus on packaging, characterisation, modelling and applications of wide-bandgap compound semiconductor power devices.

Jun Liang (M'02-SM'12) received the B.Sc. degree from Huazhong University of Science and Technology, Wuhan China in 1992, and the M.Sc. and Ph.D. degrees from China Electric Power Research Institute, Beijing China in 1995 and 1998 respectively. From 1998 to 2001, he was a Senior Engineer with China Electric Power Research Institute. From 2001 to 2005, he was a Research Associate at Imperial College, London, U.K.. From 2005 to 2007, he was a Senior Lecturer at the University of Glamorgan, Wales U.K.. Currently, he is a Professor at the School of Engineering, Cardiff University, Wales U.K.. He is the Chair of IEEE PELS UK&I Chapter. His research interests include DC technologies, power electronics, power system stability control, and renewable power generation.

Ingo Lüdtke received the Dipl.-Ing. (FH) degree in Electrical Engineering / Computer Science from Fachhochschule Braunschweig/Wolfenbï¿œttel, Germany in 1990, the Dipl.-Ing. (TH) degree in Electrical Engineering / Automation Technology from Technische Hochschule Zwickau, Germany in 1991 and the Ph.D. degree in Electrical Engineering from the University of Glamorgan, U.K. in 1998. He has received the title of Honorary Visiting Professor from Cardiff University, U.K. in 2020. His current role is Head of Power Electronics at Compound Semiconductor Applications Catapult, U.K. His research interests are in motor control, optimisation, modelling and applications of wide-bandgap compound semiconductor power devices.

Steve Berry is a principal power electronics engineer at the Compound Semiconductor Applications (CSA) Catapult, U.K where he is responsible for technical quality and delivery of collaborative R&D projects using GaN and SiC devices. He is passionate about all aspects of power conversion and has designed power converters and systems from mW to 2MW. In his 33 years experience his constant drive is to gain fundamental understanding of the devices and circuits. Previous design experience has been single and three phase UPS, high precision power supplies for superconducting magnets up to 13kA, industrial motor drives and domestic products. He received the B.Eng. Degree in Electrical and Electronic Engineering from Hatfield Polytechnic in 1988. His interests include novel bi-directional semiconductor devices and topologies, soft-switching, quasi-resonant and multi-resonant power conversion techniques. Stephen is the sole author of one patent and joint author of six patents.

Konstantinos Floros received the Ph.D. and the First Class Honours M.Eng. degrees in Electronics and Electrical Engineering from the University of Glasgow, Glasgow, U.K. He is a Power Engineer at Compound Semiconductor Applications (CSA) Catapult, working on collaborative research and development as well as on commercial projects centred around the utilisation of compound semiconductors. His research interests include wide bandgap power electronic device design, fabrication processing, device characterisation techniques, and power device applications.